Heliyon 10 (2024) e39753

Contents lists available at ScienceDirect

Heliyon

journal homepage: www.cell.com/heliyon

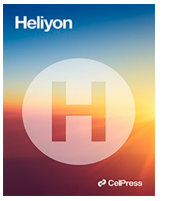

Research article

Exploring the impact of calcium phosphate biomaterials on cellular metabolism

Jingzhi Fan [a,b], Theresa Schiemer [a,b], Vita Steinberga [a], Annija Vaska [a,b], Anastasija Metlova [b,c], Antons Sizovs [b,c], Janis Locs [a,b], Kristaps Klavins [a,b,*]

[a] Institute of Biomaterials and Bioengineering, Faculty of Natural Sciences and Technology, Riga Technical University, Riga, Latvia
[b] Baltic Biomaterials Centre of Excellence, Headquarters at Riga Technical University, Riga, Latvia
[c] Latvian Institute of Organic Synthesis, Riga, Latvia

ARTICLE INFO

Keywords:
Glycolysis
Calcium phosphate
Hydroxyapatite
β-tricalcium phosphate
Metabolism

ABSTRACT

Calcium phosphate (CaP) biomaterials have been widely used in hard tissue engineering, but their impact on cell metabolism is unclear. We synthesized and characterized hydroxyapatite, β-tricalcium phosphate, and biphasic calcium phosphate composites to investigate material effects on NIH/3T3 cell metabolism. The intracellular metabolites were analyzed employing LC-MS metabolomics, and cell metabolic status was assessed comparatively. Our results revealed that CaPs adsorb metabolites, particularly amino acids. Furthermore, CaP biomaterials significantly influence amino acid and energy metabolism pathways. Specifically, we observed glycolysis and TCA cycle activity stimulation, resulting in higher energy consumption in cells adhered to CaP surfaces. Our findings suggest that CaPs composed of different ratios of hydroxyapatite (HAp) and β-tricalcium phosphate (β-TCP) have a similar impact on cell metabolism alterations. Moreover, we observed that the metabolism alterations gradually decreased over time. Our study enhances understanding of cell-CaP interplay, paving the way for metabolic regulation biomaterials and improving efficacy in tissue engineering and regenerative medicine.

1. Introduction

Bone is distinguished by its unique, organic matrix composition (35 %) and inorganic components (65 %) [1]. Calcium phosphate

Abbreviations: HAp, hydroxyapatite; CaP, calcium phosphate; β-TCP, β-tricalcium phosphate; BCP, biphasic calcium phosphates; XRD, X-ray diffraction; ANOVA, analysis of variance; F6P, fructose 6-phosphate; FBP, fructose 1,6-bisphosphate; PCA, principal component analysis; AMP, adenosine monophosphate; ADP, adenosine diphosphate; ATP, adenosine tri-phosphate; UMP, uridine monophosphate; UDP, Uridine diphosphate; UTP, uridine triphosphate; CMP, cytidine monophosphate; CDP, cytidine diphosphate; CTP, cytidine triphosphate; OMP, orotidine monophosphate; His, Histidine; Trp, Tryptophan; Tyr, Tyrosine; Phe, Phenylalanine; Gly, Glycine; Gln, Glutamine; Asp, Aspartate; Tau, Taurine; Cys, Cystine; Met, Methionine; Ser, Serine; Val, Valine; Leu, Leucine; Ile, Isoleucine; Ala, Alanine; Arg, Arginine; Pro, Proline; Cr, Creatinine; PCr, Phosphocreatine; Glucose-6P, Glucose-6-phosphate; Ribulose-6P, Ribulose-6-phosphate; Erythrose-4P, Eythrose-4-phosphate; Fructose-6P, Fuctose-6-phosphate; Sedoheptulose-1,7P2, Sedoheptulose-1,7-bisphosphate; R5P, Ribose-5-phosphate; PRPP, Phosphoribosyl pyrophosphate; DHAP, Dihydroxyacetone phosphate; GA3P, Glyceraldehyde-3-phosphate; Acetyl-CoA, Acetyl coenzyme A; PEP, Phosphoenolpyruvate; NAD, Nicotinamide adenine dinucleotide; FAD, Flavin adenine dinucleotide; GMP, Guanosine monophosphate; IMP, Inositol monophosphate; Ura, Uracil; Urd, uridine.

* Corresponding author. Institute of Biomaterials and Bioengineering, Faculty of Natural Sciences and Technology, Riga Technical University, Riga, Latvia.

E-mail address: kristaps.klavins_3@rtu.lv (K. Klavins).

https://doi.org/10.1016/j.heliyon.2024.e39753
Received 2 April 2024; Received in revised form 18 July 2024; Accepted 22 October 2024
Available online 26 October 2024

(CaP) makes up most of the bone's inorganic substance. In bone, it exists in a form analogous to the mineral hydroxyapatite (HAp) and deposits on the collagen matrix [2]. CaP ceramics are similar in composition to bone minerals, giving them excellent biological properties that stimulate osteoconduction and osteoinduction [3]. Using CaPs as implanted biomaterials has benefited countless hard tissue repairs [4]. Hydroxyapatite and β-tricalcium phosphate (β-TCP) are the most used and potent synthetic bone graft substitutes among the many calcium phosphate materials. Both are biodegradable with excellent bioactivity [5]. CaP ceramics exhibit osteoconductivity through partial dissolution in body fluids, facilitating the reprecipitation of biological apatite on their surface. This phenomenon promotes osteoblast cell adhesion, facilitating the production of the bone matrix. Nevertheless, these materials still present distinct clinical challenges, including chronic inflammation and degradation rates that do not align with tissue growth rates [6]. To achieve a better therapeutic outcome, significant efforts are dedicated to improving the physical, chemical, and biological properties of CaPs. The current focus of CaP biomaterial development is mainly on crystallography, morphology, organic/inorganic composite, and advanced preparation methods. At the same time, a deeper understanding of the biological mechanism behind CaP interactions with organisms is still in demand.

Cell-material interaction is a crucial bridge between biology and materials engineering. Gene expression, protein characterization, cell imaging, and histology, from in vitro to in vivo, are mature and widely applied to evaluate a new biomaterial [7]. However, the studies about crosstalk at the cell-material interface mainly focus on macromolecules, while the building blocks of living systems, the small molecules – metabolites - are belittled aside. Metabolites, including amino acids, lipids, sugars, and organic acids, are constantly consumed and formed in the anabolism or catabolism process to maintain cell functions [8]. The catabolic and anabolic cell activities altered by contacted materials or cellular microenvironments are directly linked to cell behaviors [9]. Therefore, metabolite profiling can be an efficient strategy for analyzing cell-material interaction. The metabolic clues can benefit the understanding and development of tissue engineering strategies [10]. On the flip side, the measurement of metabolite changes in the cellular environment has a considerable potential to directly or indirectly assess cell adhesion, differentiation, functionalization, and other cell activities. The role of metabolites in cell behaviors is getting more and more attention in biomaterial studies. Mass spectrometry-based metabolomics can acquire accurate quantitative information on metabolites and their diversity [10,11]. Mass spectrometry enables the simultaneous detection and measurement of several hundreds of metabolites, providing characteristic chemical fingerprints and offering cutting-edge technology for novel diagnostic and prognostic approaches in contemporary health and medical science research [12]. The measured cellular metabolite profiles provide information about catabolic and anabolic regulation in cell health, accurately reflecting cellular phenotype [10]. In recent years, metabolomics has become crucial in clinical research, drug discovery, nutritional science, and toxicology. Metabolomics studies are widely applied to investigate various human diseases, improve diagnosis, and design therapeutic strategies [13]. Similarly, metabolomics could be a powerful tool in advanced biomaterial research and development. The influence of CaPs on cell metabolism has not yet been fully understood. Such knowledge about cell-material interaction can aid the development of advanced bio-functional materials. Combining metabolomics with other material evaluation techniques can provide a comprehensive understanding of complex biomolecular processes.

In this study, we selected calcium phosphate-based bioceramics to study their influence on cell metabolism as they are clinically relevant and widely used biomaterials. For this purpose, bioceramics were synthesized via wet precipitation and characterized by X-ray diffraction (XRD), contact angle, and cell viability tests. The investigated materials were hydroxyapatite (HAp), β-tricalcium phosphate (β-TCP), and biphasic calcium phosphate (BCP) composites with HAp/β-TCP ratios of 95/5 w/w (named H95) and 58/42 w/w (named H58). The two HAp/β-TCP ratios have been approved on the market and clinically applied (e.g., Calciresorb™ and CellCeram™) [14]. Different ratios were included to verify whether BCP composition affects metabolism.

We selected the NIH/3T3 fibroblasts cell line for the model cell culture as these cells are commonly used as cell-material interaction models to characterize biomaterials [15]. Cells were cultured on calcium phosphate (CaP) materials for 5 days. Quantitative metabolite profiles were determined using LC-MS-based workflow, and statistical analysis was applied to compare the metabolite profiles between different groups. Besides the intracellular metabolite profile, the metabolite adsorption on CaP materials was also investigated.

We were able to demonstrate that CaPs can adsorb metabolites. Moreover, CaPs altered cellular amino acid metabolism and accelerated energy metabolism, and the CAP's influence on cell metabolism decreased over time. The results expand the current understanding of CaP-based bioceramic interactions with cells and demonstrate the applicability of metabolomics in biomaterials research.

2. Material and methods

2.1. CaP materials preparation

Calcium phosphate powders were synthesized via the wet precipitation synthesis described by Sokolova1 et al. [16] In brief, calcium oxide (CaO, Fluka, from marble, ≥97 %), orthophosphoric acid (H_3PO_4, Sigma-Aldrich, 85 % w/w), and deionized water were used in the wet precipitation reaction. The pH of the reaction media varied between 5.0 and 7.6, depending on the desired phase composition of the product. Generally, an acidic pH for the β-TCP phase and an alkaline pH for the HAp phase were set. The precipitates were washed, vacuum-filtered, and dried. Detailed description of procedures is available in supporting information (Synthesis of CaPs). The obtained powders were pressed into CaP discs under the pressure of 30 KPa and further sintered with high temperatures to produce disks that fit the 24-well plate for cell culture. The temperatures for sintering were as follows: HAP: 990 °C; H95: 1030 °C; H58: 1135 °C; TCP: 1100 °C. The materials were sterilized by autoclaving at 121 °C for 20 min. A contact angle test was applied to the sintered CaPs to assess the surface hydrophobicity. 10 ml of deionized water was dropped onto material surfaces and captured by a

camera. The angles were measured using ImageJ software.

2.2. The pH and ion release test

The pH test and calcium and phosphate ion release test from the materials were conducted using Dulbecco's Modified Eagle's medium (DMEM, Gibco) by immersing CaPs disks for 24 h (1 ml/disk). The pH was measured by pH meter (WTW inoLab pH 7110). The calcium level in media was measured by calcium colorimetric assay kit (Sigma). 50 μL conditioned media was taken into the 96-well plate (Tecan), followed by 90 μL of the chromogenic reagent to each well. 60 μL calcium assay from buffer supplied from the assay kits. The plate was incubated at room temperature for 15 min, protected from light, and then immediately measured by the plate reader (Tecan), with the absorbance at 575 nm. The phosphate level in media was measured by phosphate assay kit (Sigma). 50 μL conditioned media was taken into the 96-well plate (Tecan), followed by 100 μL of the malachite green reagent to each well. The plate was incubated for 30 min at room temperature, avoiding light interference. The plate reader (Tecan) set to the absorbance at 620 nm was employed for measurements.

2.3. Scanning electron microscope (SEM) imaging

After incubation for 24 h, the NIH/3T3 cells were rinsed with phosphate-buffered saline (PBS). Samples were washed twice with PBS (37 °C) and fixed in 4 % paraformaldehyde solution for 40 min at room temperature. Then, cells were washed three times with cold PBS and dehydrated with gradual ethanol dehydration (25 %, 50 %, 75 %, 90 %, 100 %; 5 min each) and dried for 20 min after adding one drop of hexamethyldisilane (Sigma Aldrich, $\geq$99 %) on top of the material. The original CaP materials were imaged together with the cells on materials by SEM. Dried materials were mounted on sample holders with double-sided carbon tape and sputter coated with carbon (LEICA EM ACE200, Flash, 20 pulses), and one connective line was drawn with silver paint. SEM images were acquired at 5 keV, 1 uS scanning speed, and a distance of 3.03 mm (Tescan Vega SEM) using frame averaging with 50 frames.

2.4. Specific surface area analysis

The results were calculated using the Brunner-Emmett-Teller (BET) specific surface area theory. The surface area was measured with the N_2 adsorption system QuadraSorb SI (Quantachrome Instruments, USA). All material tablet samples were broken into pieces to fit the container. Excess moisture and vapors were removed at room temperature for 24 h.

2.5. X-Ray diffraction (XRD) characterization of CaPs

The crystalline phase of all sintered CaP discs was determined by XRD (PANalytical Aeris, Netherlands) to verify the composition of CaPs. The characterization analysis was performed with X'Pert Data Collector, X'Pert Data Viewer, X'PertHighScore, and the International Centre for Diffraction Data PDF-2 (ICDD). XRD patterns were recorded using 40 kV and 15 mA, K-α1,2 wavelengths 1.541, step size 0.0435°, within range 2θ from 10° to 70°, time per step 147.39 ms, for crystalline phase identification succeeding ICDD entries were used. The crystallographic patterns and corresponding peaks of HAp (ICDD 09-0432) and β-TCP (ICDD 09-0169) were identified using X'PertHighScore software (Malvern Panalytical, Worcestershire, UK), based on data from the International Center for Diffraction Data (ICDD) database. Detailed instrument settings are given in Table S3. Crystallographic identification of the synthesized phases was accomplished by comparing the experimental XRD patterns to ICDD.

2.6. Cell culture and viability tests

NIH/3T3 cell line (ATCC CRL-1658, ECACC 93061524), (6×10^4 cells/ml) were cultured in Dulbecco's Modified Eagle's medium (DMEM, Gibco) supplemented with 10 % calf serum (Sigma-Aldrich) and 1 % Penicillin-Streptomycin (Gibco). The cells were incubated at 37 °C in a 5 % CO_2 environment. The cells at passage 7 were seeded on material surfaces in a 24-well culture plate with 4 replicates of each group. The cells seeded in wells without materials were used as control groups. Metabolite extraction was performed for all the cells on days 1, 3, and 5 for 4 replicates per group and time point. Cell Counting Kit-8 (CCK-8, Sigma-Aldrich) was used to determine cell viability in parallel with 4 replicates in each group. Mycoplasma from culture media was tested by Rapid Mycoplasma Detection Kit (AssayGenie) and shown negative.

2.7. Cell attachment analysis

Materials were placed in a 24-well plate, and 3×10^4 cells were seeded in 100 μl and left to attach. The culture medium (supernatant) and the cells on the materials were pipetted out for further cell viability tests. Per the manufacturer's instructions, viability was assessed in duplicates using CellTiter-Blue (Promega).

2.8. Metabolite extraction

The methanol-based protocol was employed for the metabolite extraction. It was essential to extract cells directly from the material to avoid changes in cell metabolism during detaching. Before the extraction, cell culture media was removed, and cells were washed

with ammonium bicarbonate (NH_4HCO_3, Sigma-Aldrich, ≥99.5 %) solution (75 mM, 37 °C). Cells were then quenched in cold 80 % v/v methanol (CH_3OH, Sigma-Aldrich, ≥99.9 %) and harvested by scraping. The harvested samples were centrifuged at 600 RCF at room temperature for 5 min, and the supernatant was collected. The collected supernatant was dried by vacuum centrifuge. Afterward, 10 μL of the isotopically labeled internal standard mix was added to dried samples, followed by 90 μL of methanol. Reconstituted samples were transferred to glass vials and used for liquid chromatography-mass spectrometry (LC-MS) analysis.

The same metabolite extraction procedure was also applied to the CaPs without cultured cells to verify the adsorption of metabolites by materials. 1 ml complete media was filled in well plates with and without materials for 24 h, and 3 replicates were set for each group. The media was removed, the wells were washed with ammonium bicarbonate solution, and cold 80 % v/v methanol was added. The methanol solution was collected by pipetting and scraping. The extracts were dried by vacuum centrifuge, and 10 μL of the isotopically labeled internal standard mix was added to dried samples, followed by 90 μL of methanol. Reconstituted samples were transferred to glass vials and used for liquid chromatography-mass spectrometry (LC-MS) analysis.

2.9. Metabolite analysis

Targeted quantitative metabolite analysis was conducted using HILIC-based liquid chromatography combined with mass spectrometric detection employing a triple quadrupole mass spectrometer. Metabolites were separated on an ACQUITY UPLC BEH Amide 1.7 μm 2.1 × 100 mm analytical column (Waters). The gradient elution was carried out using 0.15 % formic acid and 10 mM ammonium formate in water as mobile phase A and a solution of 0.15 % formic acid and 10 mM ammonium formate in 85 % acetonitrile as mobile phase B. The initial conditions were set to 100 % mobile phase A. After 6 min, a 0.1 min gradient (6.0–6.1 min) was started, and the mobile phase A level was reduced to 94.1 %. From 6.1 to 10 min, mobile phase A was set to 82.4 %, and from 10 to 12 min, mobile phase A was set to 70.6 %. The column was then equilibrated for 6 min at initial conditions. The total analysis time was 18 min. The mobile phase flow rate was 0.4 mL/min; the injection volume was 2 μL, and the column temperature was 40 °C. For MS detection, a TSQ Quantis (Thermos Fisher Scientific) triple quadrupole mass spectrometer was used. The MS analysis was performed in ESI positive and ESI negative modes using MRM detection (MRM settings are provided in Supplement Information). The ESI spray

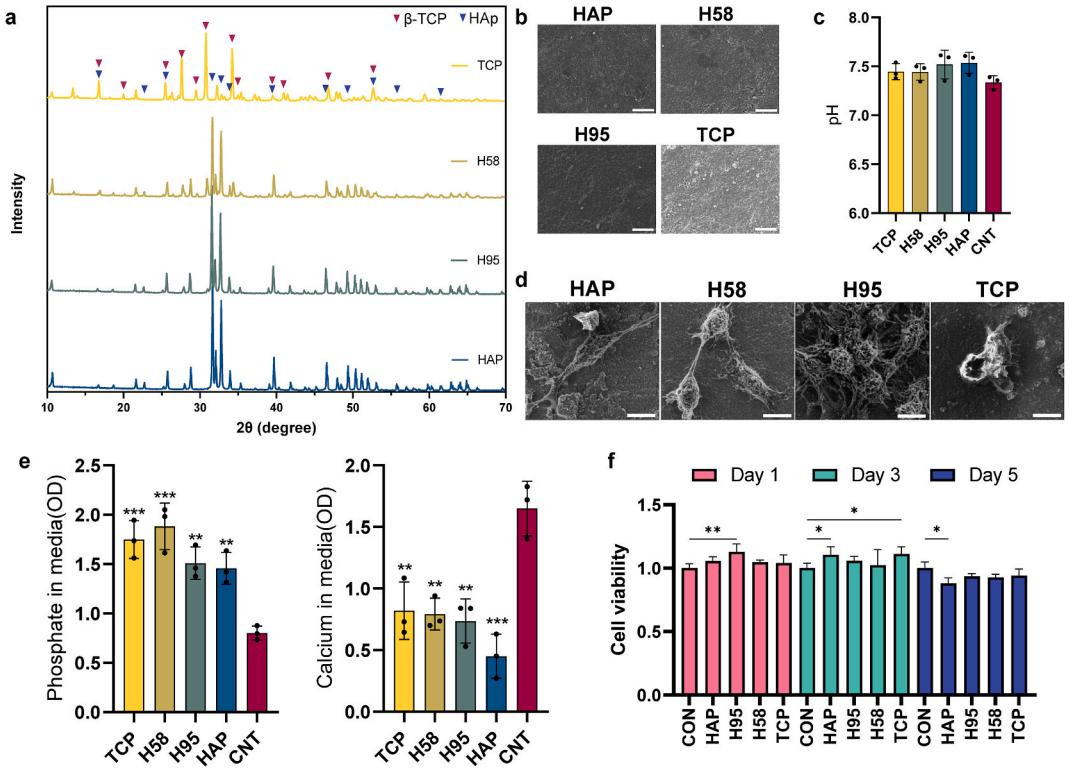

Fig. 1. a) The XRD analysis of CaP disk crystal structure. Red arrows indicate characteristic peaks of β-TCP, and blue arrows indicate distinct peaks of HAp. The composites had both patterns, and the peak values varied by the compositions. The intensity and pattern of corresponding peaks changed according to the relative composition ratio of HAp/β-TCP. Peaks at 27.80° (214), 31.07° (210), and 32.42° (128), 34.23° (220), indicating the increase of the HAp phase proportion. b) SEM images of prepared CaP disks. Scale bar = 10 μm c) pH of media immersed with materials. d) The SEM images of cells attached to CaP material surfaces. Scale bar = 10 μm. e) Phosphate and calcium ion level of media immersed with materials. $^{**}P < 0.01$, $^{***}P < 0.001$ v CON. f) The cell viability was tested by CCK-8 on days 1, 3, and 5. Cell viability is normalized to control samples. Synthesized CaPs significantly increased cell viability compared to controls (one-way ANOVA followed Tukey's multiple comparisons tests, $^{*}P < 0.05$, $^{**}P < 0.01$ vs. CON).

voltage was set to 3.5 kV in positive mode and 2.5 kV in negative mode, the gas heater temperature was set to 400 °C, the capillary temperature was set to 350 °C, the auxiliary gas flow rate was set to 12 arbitrary units, and nebulizing gas flow rate was set to 50 arbitrary units. For quantitative analysis, seven-point calibration curves with internal standardization were used. Tracefinder 51.1 General Quan (Thermofisher Scientific) software was used for LC-MS data processing and quantification. Detailed information of detected metabolites is shown in Table S4. The metabolite concentration was normalized for further data analysis versus cell counting results.

2.10. Data analysis

The metabolomics data analysis was performed with MetaboAnalyst 5.0 [17]. The total amount of metabolites was normalized based on the number of cells according to the cell proliferation data. For data preprocessing, obtained concentrations were log-transformed and scaled by mean-centering, and each variable was divided by the standard deviation. GraphPad Prism 9 was used for statistical analysis. The metabolites with a high adsorption rate (fold change over 0.1 compared to the cell results) were excluded from the group comparison. Analysis of variance (ANOVA) was applied for multi-group data. Pathway enrichment analysis used The Small Molecule Pathway Database as the pathway library. Fold-change and p-value were calculated for two-group comparisons to find significantly changed metabolites. The two-group comparison data was analyzed using the *t*-test. The cluster analysis was performed by principal component analysis (PCA). The machine learning method to rank the metabolite contributions to classification accuracy was done by random forest, with 500 trees and 7 predictors.

3. Results

3.1. Characterization of CaP materials

The hydrophilicity test was conducted and presented by the contact angle (Supplemental information, Fig. S1). The angles were 91.781 (TCP), 92.278 (HAP), 95.020 (H95), and 90.944 (H58). The samples had a mild hydrophobicity, which was acceptable for cell cultures, and no significant difference between different CaP samples was observed.

XRD was used to determine the composition of sintered CaP discs (Fig. 1a). Pattern fitting was carried out between 10° and 70°. The diffraction patterns showed sharp diffraction peaks, indicating the presence of different crystalline species in CaP discs, including β-TCP and HAp. The materials were verified as pure HAp, β-TCP, and BCP with HAp/β-TCP ratios of 95/5 and 58/42. The Ca/P ratio of prepared CaPs are presented in Table 1.

$$\text{Overall Ca} \,/\, \text{P ratio} = \omega_{\beta-\text{TCP}} \times 1.5 + \omega_{\text{HAp}} \times 1.67$$

SEM was used to characterize the morphology of 4 types of CaP disks (Fig. 1b). The material had a slightly rough but relatively flat surface. Ceramic materials sintered at high temperatures had a high degree of sealing on the surface. Cells (about 10 μm) cannot enter the material's interior but can only grow on the surface.

The material did not cause pH changes in the culture medium (Fig. 1c). In the absence of cells, immersion for 24 h reduced the calcium concentration of the culture medium. On the contrary, the concentration of phosphate ions is increased by the biomaterial (Fig. 1e). The addition of CaPs could cause precipitation of calcium phosphate compounds. This lead to a decrease in the free calcium ion concentration in the media as calcium ions bind to phosphate ions and precipitate out of solution.

3.2. Cell viability and attachment

Cell viability responding to a biomaterial is a critical parameter commonly assessed during biomaterial evaluation. Furthermore, for quantitative metabolite analysis, different cell numbers can influence quantitative results; hence, it is crucial to normalize obtained data to the cell numbers. The CCK-8 measures the metabolic activity of cells by reacting with NAD(H) and NADP(H), therefore reflecting the total number of viable cells. The cell viability for material groups was similar to the surface-treated culture plate (Fig. 1f). As expected, CaPs showed good biocompatibility, and cell viability was not affected when seeded directly on material surfaces. SEM images and cell attachment analysis showed attachment and cell spreading (Fig. 1d and Fig. S2.). The cell viability and attachment results confirmed the quality of the synthesized CaP materials in this study.

Table 1
Ca/P ratio. The crystal form ratio is calculated from the XRD analysis results using the formula: Overall Ca/P ratio=ωβ−TCP×1.5+ωHAp×1.67.

Materials	Overall Ca/P ratio
HAp	1.67
H95	1.66
H58	1.60
TCP	1.50

3.3. Intracellular metabolic profiling

We employed a targeted quantitative metabolomics approach in this study and analyzed 58 metabolites. Broadly, those metabolites fall into 6 related categories: TCA cycle, glycolysis, pentose phosphate pathway, nucleotide synthesis, fatty acid oxidation, and amino acid metabolism. The downstream analysis of obtained metabolite data was divided into three parts: in-between CaP materials, between CaPs and the control group, and analysis of longitudinal metabolism changes. The obtained quantitative metabolite values were log-transformed, scaled by mean-centering and presented in a heatmap (Fig. 2).

3.4. Metabolites adsorption by CaPs

Understanding the influence of metabolite adsorption is vital as it can alter the cellular microenvironment. Moreover, considering the potential adsorption of metabolites onto biomaterial surfaces from cell culture media is essential to address experimental biases, as co-extraction with intracellular metabolites may compromise the accuracy of the results. In this study, we focused on intercellular metabolite measurements. Therefore, evaluating if the experimental condition could introduce bias in metabolite measurements was essential to ensure accurate data interpretation. The experimental procedure included immersion of the cap disk in cell culture media, seeding the cell directly on the material, and extracting the intercellular metabolites. Typical cell culture media contains a plethora of metabolites to ensure proper cellular functions. These small molecules can adhere to biomaterial surfaces and could be co-extracted with intercellular metabolites, resulting in inaccurate metabolite data. To assess the metabolite affinity for adsorption on material surface and thus potential interferences when analyzing intercellular metabolite levels, we performed metabolite extraction for CaP disks immersed in complete media containing 90 % DMEM and 10 % calf serum without cells. 29 metabolites were found to adsorb onto the CaP surface even after washing with PBS (Fig. 2). Compared to the control (cell culture plate), more metabolites were adsorbed onto CaP surfaces. CaPs showed a higher affinity with the positively charged amino acids (basic side chains). Lactic acid was adsorbed on both CaP and control groups, while the lactic acid level on the CaP surface was almost 4 times lower than the control (on the plate). Sulfur-containing amino acids (methionine, taurine, and cystine) had the highest adsorption affinity on CaP surfaces. Both CaP and culture plate showed attraction to arginine.

To assess the impact of adsorption on extracted metabolite levels, the quantities of adsorbed metabolites were compared with intracellular metabolite levels. This analysis aimed to determine how much adsorption influenced the measured metabolite levels. For this purpose, the average concentration of metabolites from the biomaterials group on day 1 was used as a reference to calculate fold changes of the CAP group, and the control group was calculated with the intracellular metabolites of the control group (without biomaterial) from day 1. 26 metabolites had a high adsorption rate (fold change over 0.1 compared to the cell results) (see Fig. 3).

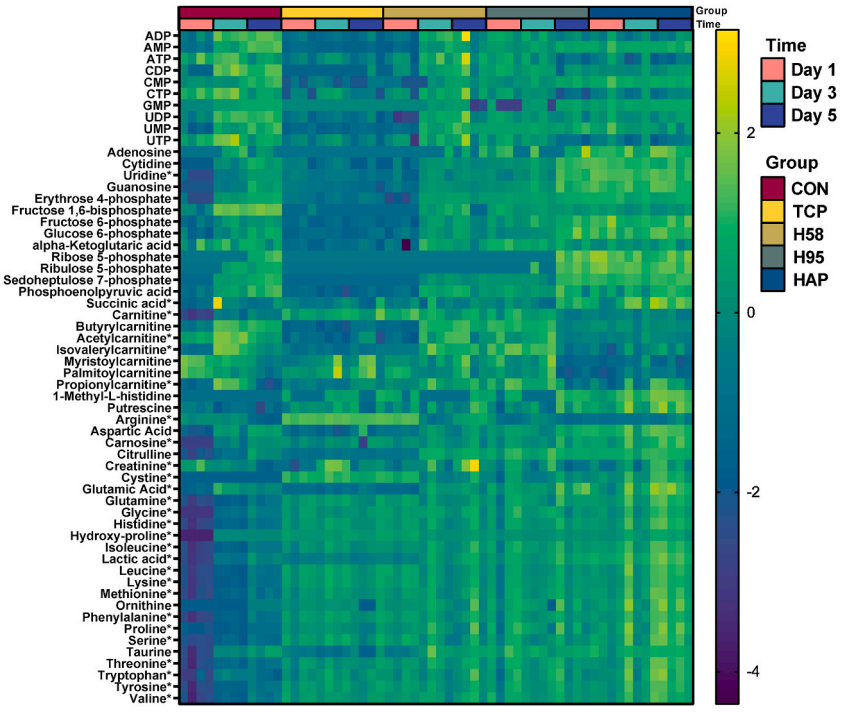

Fig. 2. The heatmap of the complete metabolite profile for 5 groups at 3 different time points. Metabolites are nucleosides, sugar metabolites, carnitine family, and amino acids. Metabolites that adsorbed on CaP surfaces are labeled by *.

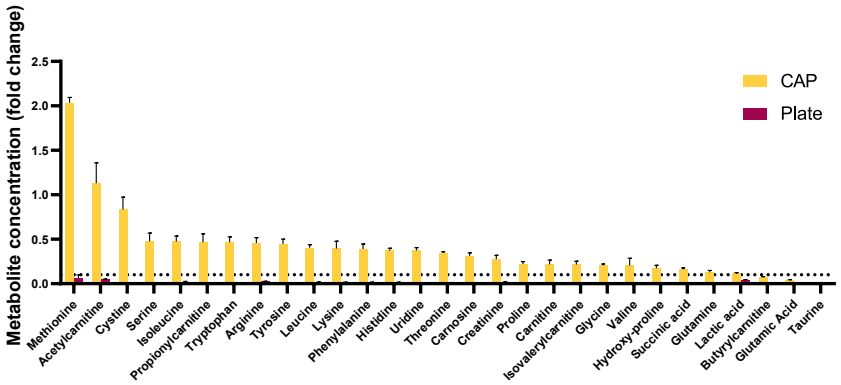

Fig. 3. The level of metabolites adsorbed onto calcium phosphate surfaces and culture plate surfaces. The levels were compared to intracellular metabolite levels and expressed as fold change. The group to compare was a 24-well culture plate (Purple color, material PS, surface treated), and for intracellular metabolite levels, average values for the materials group collected on day 1 were used. Metabolites with a high adsorption rate (a fold change greater than 0.1 compared to the intracellular results) were excluded from further analysis.

3.5. CaP material phase composition influence on cell metabolism

We used PCA and ANOVA to investigate if CaP phase composition influenced metabolite levels. No distinct clusters for CaP samples with various phase compositions were observed with PCA. (Fig. 4). With ANOVA, in all 3 days the residuals presented a normal distribution (Supplemental information, Fig. S3). To follow up on a potential correlation with hydroxyapatite content, we performed the pattern search between CaPs (Supplemental information, Fig. S5), i.e., correlate metabolite changes to HAP phase content (0, 58 %, 95 %, and 100 %). Although few metabolites were found to increase or decrease with the changes in HAp content, the correlation coefficients were too low to draw any conclusions.

3.6. CaP biomaterials influence cell metabolism

Glycolysis was the most significantly changed one from pathway enrichment analysis, followed by other energy metabolism pathways and gluconeogenesis fructose and mannose degradation (Fig. 5a). Statistical data analysis, including PCA and *t*-test, was performed to identify metabolites with significant changes induced by CaP bioceramics. PCA score plots revealed a close clustering of the CaP materials group and a substantial separation between the materials group and the control group (Fig. 5d). The metabolite levels at the earlier time point had significantly higher variation compared with the later time points, suggesting a more substantial distinction between CaPs and control groups at the initial phase of biomaterials exposure (Fig. 5c). Proline level was up to 5 times higher in CaP groups over all 3 time points. Notably, the reduction of any amino acid was not observed with CaP groups. On the other hand, levels for compounds involved in energy metabolism were significantly lower upon exposure to CaPs (Fig. 5b). For example, ATP levels in material groups were 4 times lower than the control groups (Fig. 5e). At the same time, levels of fructose 1,6-bisphosphate (FBP), a critical molecule in the glycolysis metabolic pathway, were 10 times reduced in cells exposed to CaPs (Fig. 5e).

3.7. Analysis of metabolism changes over time

Metabolism is a dynamic process. Therefore, we extracted metabolites at 3-time points to obtain data about temporal CaP's influence on cell metabolism. PCA score plot (Fig. 6a) showed a clear separation of material and control groups for all time points. However, the distance between the groups on the PC1 axis diminishes over time.

We found compounds of energy metabolism (G6P, F6P, FBP, and lactic acid) and nucleotides (ATP and ADP) significantly altered with prolonged CaP exposure time. The level of nucleobase adenosine was rapidly increased, whereas the taurine level was gradually reduced, and fold change compared to control decreased from 4 on day 1–1.2 times on day 3.

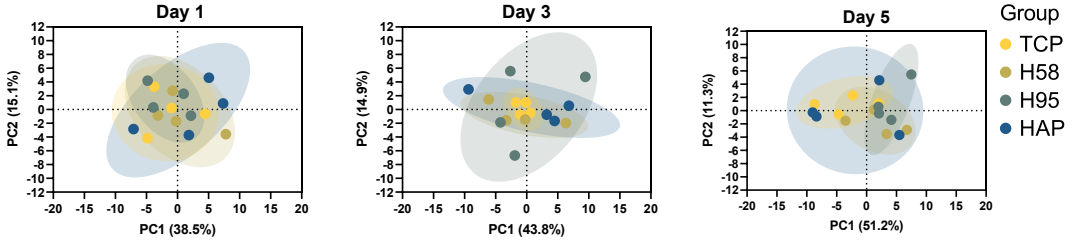

Fig. 4. PCA plots of all 4 types of CaPs on Day 1, Day 3, and Day 5.

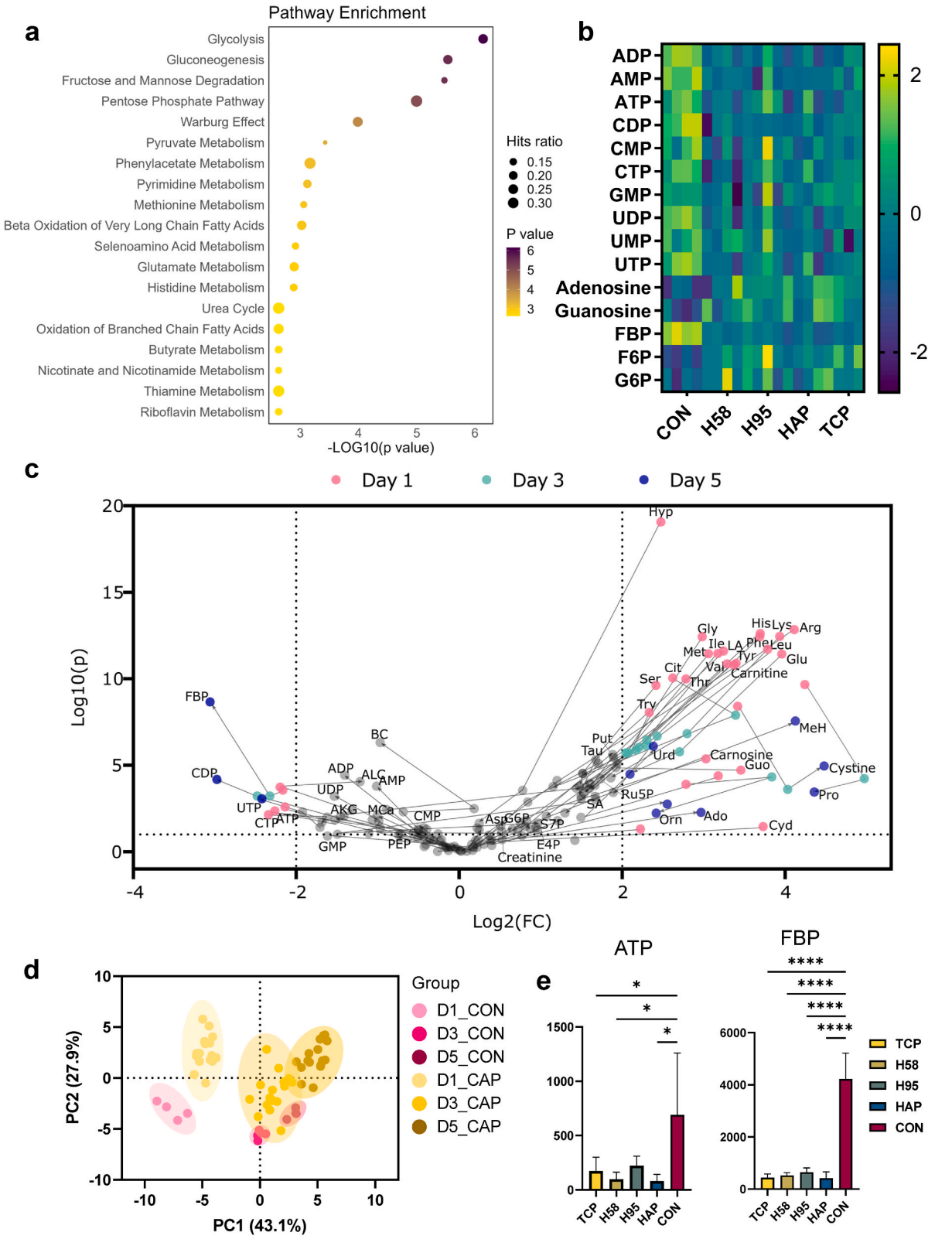

(caption on next page)

Fig. 5. a) Pathway enrichment analysis b) The heatmap of nucleotides and pentose phosphate pathway/glycolysis metabolites on day 1. c) The volcano plot of metabolites. Lines in the volcano plot link the significant metabolites on different days. The lines provided clues about the direction of changes and the metabolite's ability to distinguish between the material and control groups. Thresholds: log2 (fold change) > 2 or < -2, and -log10(p) > 1. Fold change was calculated from CON for each metabolite, fold change = (metabolite level in CaP)/(metabolite level in CON). d) PCA for all CaP and control groups from days 1, 3, and 5 (n = 4). e) The metabolite level of ATP and FBP from each group on day 1. *$P < 0.05$, & $P < 0.0001$ (n = 4).

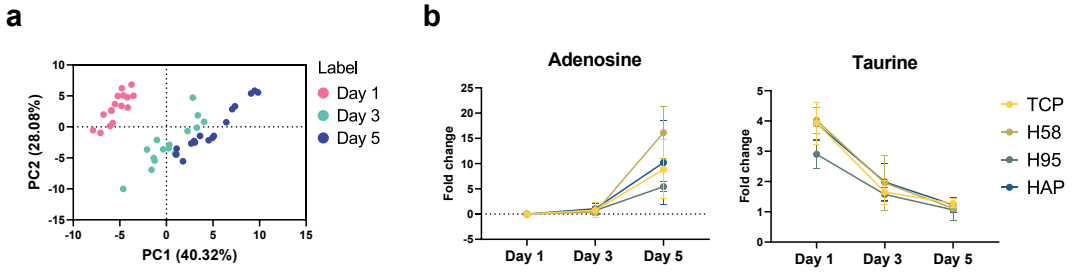

Fig. 6. a) The PCA plot scores of intracellular metabolites from material groups on days 1, 3, and 5. b) The fold changes of adenosine and taurine over time. n = 4.

The metabolic alteration caused by CaPs during the 3-time points was compound-specific. Some metabolites indicated a trend toward narrowing the disparities between CaP groups and control groups, approaching that of the control groups (Figs. 6b and 7). Among these, the difference in carbohydrate metabolism was more profound (Fig. 7). Levels of G6P and F6P initially were close to the control and increased over time. FBP was exhausted on the first day. Although FBP increased over time, the level was still lower than

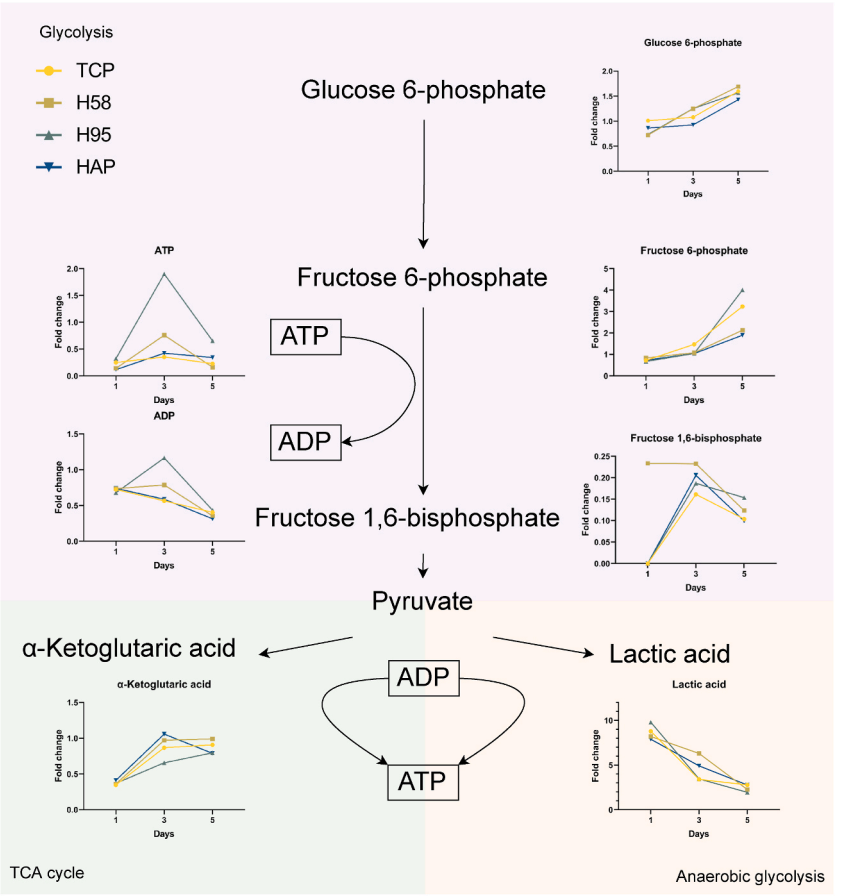

Fig. 7. The changes of metabolite levels in glucose metabolism.

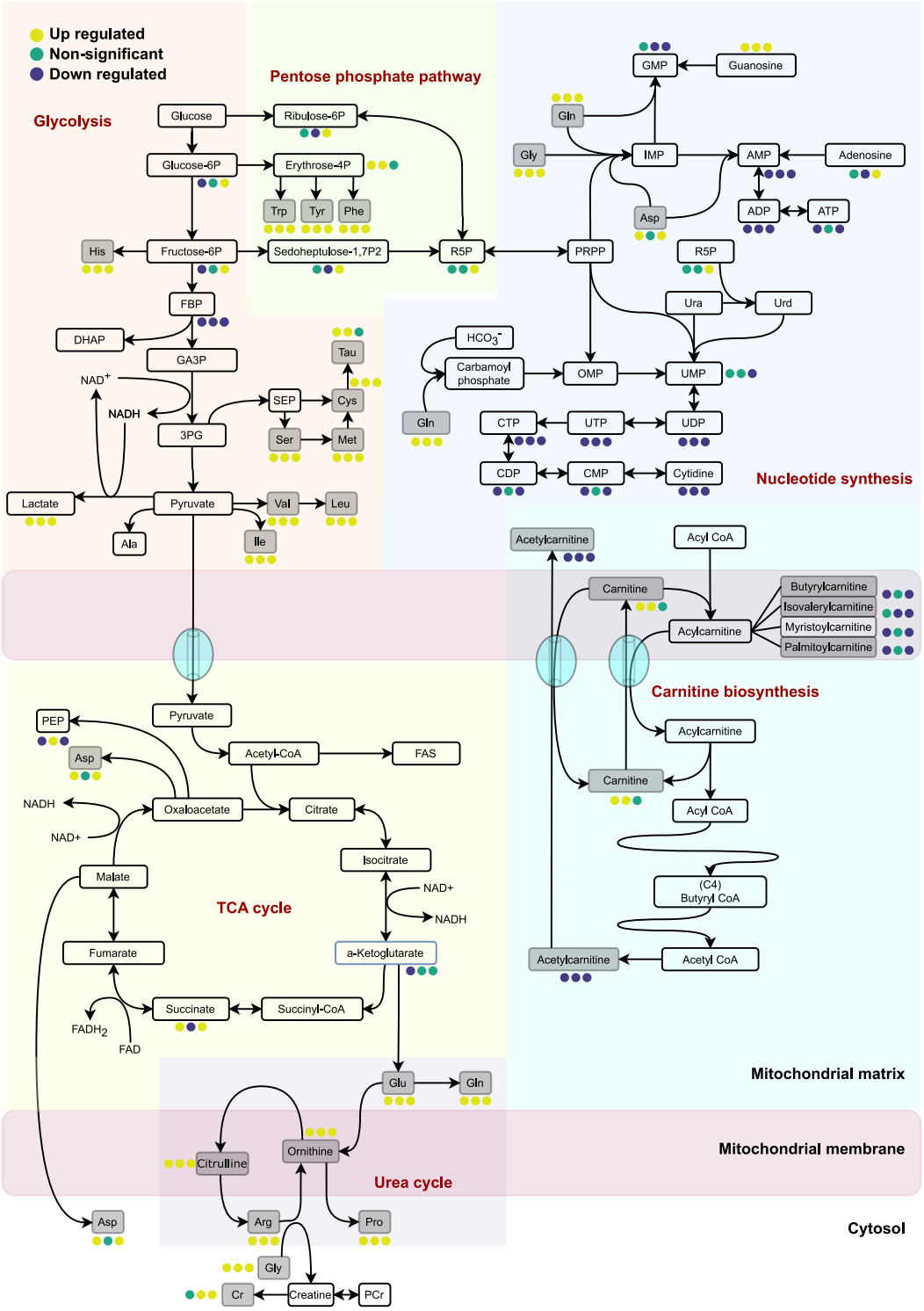

Fig. 8. The metabolic pathway map of detected metabolites. Metabolites were marked as up/down regulated or non-significant changes by color code. The covered pathways include glycolysis, the pentose phosphate pathway, nucleotide synthesis, the TCA cycle, carnitine biosynthesis, and the urea cycle.

the control. ATP had dynamic changes, and ADP slightly decreased over time. Also, on the first day, α-Ketoglutaric acid was about half the amount of the control, and lactic acid was 9 times higher than the control. Both of these subsequent metabolites were steadily approaching the control. α-Ketoglutaric acid, a key metabolite in the TCA cycle, was increasing, while lactic acid, a final product of anaerobic glycolysis, was decreasing (see Fig. 8).

4. Discussion

Despite the prevalent use of CaP-based biomaterials in clinical applications, their impact on cell metabolism remains understudied. We aimed to explore the cellular perturbations induced by calcium phosphates. In this study, we focused on three aspects: (I) metabolite adsorption on biomaterials, (II) biomaterial influence on cell metabolism, and (III) longitudinal changes in cell metabolism.

Metabolite adsorption on biomaterials is crucial in metabolism studies, as it can impact measured intracellular concentrations due to co-extraction with cellular metabolites. Adsorbed metabolites on material surfaces enhance their availability to cells, potentially modulating microenvironment and cellular functions. Our results showed an increased affinity of several compounds toward CaPs. Cystine is excessively adsorbed on CaP ceramics. Cystine is the oxidized and predominant form of cysteine in non-reducing environments, such as the extracellular space [18]. Our results suggest that the CaP ceramic surfaces provide a reducing extracellular environment to cells via the adsorption of oxidized metabolites. This aligns with numerous reports noting high cell viability on CaPs, suggesting that their physicochemical properties mitigate oxidative stress. Besides cysteine, other amino acids were adsorbed by CaPs. Notably, the amino acids with basic side chains (His, Lys, and Arg) adsorbed to CaPs at a higher level. The hydroxyl group from CaPs attracts the amino acids by interacting with the amino groups (Gln) or carboxy (Ser, Trp, and Tyr). Carnitine and its metabolites are also adsorbed on CaP surfaces utilizing similar interactions. Carnitine's function in cells is to transport fatty acids into the mitochondria, indicating that cells that come into contact with CaPs have altered energy metabolism [19]. Taurine, a sulfur amino acid with diverse biological functions, adsorbs on CaP surfaces by its amino group, and there was no trace of taurine on the culture plate surface. Taurine substantially impacts energy metabolisms [20]. The ability of biomaterials to adsorb small molecules can be utilized in future research to develop advanced biomaterials that modulate cellular phenotypes by altering the microenvironment.

Our results showed that the intracellular metabolite profiles did not significantly differ for materials with various CaP compositions. For decades, CaPs such as HAp and β-TCP have been employed in bone tissue repair, demonstrating satisfactory clinical performance [21]. While differences in properties like degradation rates are well-documented, the impact of these CaP materials on cell metabolism at the molecular level appears comparable. The differences between materials, such as degradation and hard tissue regeneration rates, are usually reported over several weeks [22]. Here, we exposed cells to CaPs for 5 days, which might not be sufficient to capture material composition-induced differences in cell metabolism. Therefore, for further data analysis, we merged results obtained from CaP groups and focused on the general perturbations caused by the material.

The results showed that CaP strongly influenced central carbon metabolism and interconnected pathways, including amino acid metabolism, glycolysis, tricarboxylic acid (TCA) cycle, and nucleotide metabolism. Intracellular amino acid levels were increased upon exposure to CaPs, including the amino acids not adsorbed on material surfaces: citrulline, aspartic acid, and ornithine. This hints that the exposure to CaPs provided the stimulus for increased amino acid biosynthesis. Arginine, hydroxyproline, and proline levels were significantly increased at all investigated time points. These amino acids are interconnected with numerous metabolism pathways [23].

A substantial disturbance of energy metabolism and higher energy consumption of the cells caused by CaPs was presumed. The levels of G6P and F6P, two intermediates of the glycolysis pathway formed in the first and second steps, respectively, were higher than the control. In contrast, the FBP, formed at the sixth step of glycolysis, was significantly downregulated by CaPs (Fig. 7.). The enzyme that catalyzes the irreversible conversion of F6P, phosphofructokinase-1 (PFK-1), is the rate-limiting enzyme of glycolysis [24]. The significant reduction of FBP indicates that glycolysis and the following energy metabolisms are extensively enhanced. As a result, the depletion of FBP could be a signature of CaP biomaterials instructing the energy metabolism switch. FBP can also indirectly alter lactic acid production by influencing glucose metabolism, especially glycolysis [25,26]. A low FBP and high lactic acid levels can result from increased glycolysis. Consequently, in pathway analysis, the most prominent alterations were observed in glycolysis, indicating a potential shift in glucose utilization for energy production. Moreover, the impact extended to various interconnected pathways, including amino acid metabolism, suggesting a broad-reaching effect on cellular functions. The perturbations observed in gluconeogenesis and fructose degradation pathways hint at alterations in carbohydrate utilization and the potential rerouting of these substrates within the metabolic network.

Amino acids and sugars are essential raw materials for the synthesis of nucleotides. For example, purine synthesis requires glycine, aspartic acid, and one-carbon units from amino acid metabolism [27]. Despite the high substrate level, CaPs significantly impair nucleotide synthesis, particularly the purine nucleotide cycle, as evidenced by a drastic reduction in the total amount of nucleotides, despite the precursor fructose 6-phosphate (F6P) being metabolized to ribose 5-phosphate via the pentose phosphate pathway [28–30].

The chemical composition of CaPs themselves modulates the cellular microenvironment by releasing calcium and phosphate ions and affecting cellular functions [31]. Low calcium concentrations have been reported to enhance cellular energy transduction, modulating three TCA cycle dehydrogenases (pyruvate, isocitrate, and α-ketoglutarate) [32]. Simultaneously, phosphate ions contribute phosphoryl groups for various cellular processes, where phosphorylation, a reversible reaction, regulates protein activity [33]. Oxidative phosphorylation in ATP synthesis involves phosphate group participation, aligning with the enhanced phosphorylation induced by CaP biomaterials. ATP and other nucleotides store and transfer chemical energy within the cell, vital for cell proliferation [34]. Our results showed that the nucleotide concentrations were significantly decreased. Activated cells with a high

phosphorylation level consume more energy, while energy metabolism was notably regulated because of the interaction with CaP. Depleted ATP and glycolytic metabolite levels indicated the metabolic impact on energy consumption and pathway regulation.

We noted diminishing metabolic disparities between CaP and the control group over time (Fig. 6a). This trend is particularly notable for lactic acid and acetylcarnitine levels (Fig. 6c). A shift in cellular energy utilization was evident across the 5 days. Initially, lactic acid levels were approximately ninefold higher than the control, decreasing by nearly half on day 5 (Fig. 7). Which indicates that early exposure to CaPs heightened anaerobic glycolysis. Simultaneously, the α-ketoglutaric acid level was reduced by half compared to the control level but reached near equivalence by day 5. The enzymatic production and reduction of α-ketoglutarate are irreversible, making it a valuable indicator of TCA cycle activity [35–37]. α-ketoglutarate decarboxylase is a rate-limiting step of the TCA cycle [32]. The depletion of α-ketoglutarate on the first day indicated a high energy consumption requirement from the TCA cycle suggesting that the cells are actively dividing and proliferating; this phenomenon suggests enhanced anaerobic glycolysis, typically observed when the TCA cycle cannot meet energy demands or under limited oxygen supply conditions.

The initial exposure to CaPs resulted in a shock pressure on the cellular energy metabolism response to biomaterials with stronger glycolysis, presented by more extensive variability in metabolite profiles. At a later time point, the metabolic alteration diminished, tending towards cellular homeostasis, which demonstrated the ability of cells to adapt to a new environment caused by CaP.

5. Conclusion

We demonstrated that calcium phosphates significantly influenced cell metabolism and the cellular microenvironment. These synthesized CaPs absorbed small molecules, particularly amino acids, affecting amino acid levels and energy pathways, notably glycolysis. Different HAp and β-TCP ratios in CaPs showed similar impacts on cell metabolism. Cells interacting with CaP surfaces displayed increased energy consumption due to heightened glycolysis and TCA cycle activity, gradually declining over time. These insights deepen our understanding of cell interactions with CaPs, shedding light on their clinical performance and opening new avenues for novel biomaterials capable of regulating metabolism.

6. Limitations of the study

This study's primary limitation lies in using fibroblasts as the model cell line instead of bone-specific cells like osteocytes or osteoblasts, which would be more relevant for bioceramic materials research. Using bone cells could yield a more clinically relevant understanding of the molecular mechanism alterations induced by biomaterial. Additionally, expanding the number of analyzed metabolites could enhance the depth of analysis.

CRediT authorship contribution statement

Jingzhi Fan: Writing – original draft, Investigation, Formal analysis, Data curation, Conceptualization. **Theresa Schiemer:** Writing – original draft, Methodology, Investigation, Formal analysis. **Vita Steinberga:** Methodology, Investigation. **Annija Vaska:** Methodology, Investigation, Formal analysis, Data curation. **Anastasija Metlova:** Methodology, Investigation, Data curation. **Antons Sizovs:** Supervision, Data curation, Conceptualization. **Janis Locs:** Supervision, Methodology, Funding acquisition. **Kristaps Klavins:** Writing – review & editing, Supervision, Project administration, Methodology, Conceptualization.

Ethics approval and consent to participate

The manuscript does not include experiments on animal or human subjects such that no ethical approval is needed.

Data availability statement

Data will be made available on request.

Declaration of competing interest

The authors declare that they have no known competing financial interests or personal relationships that could have appeared to influence the work reported in this paper.

Acknowledgment

The authors acknowledge financial support from the European Union' Horizon 2020 research and innovation program under the grant agreement No. 857287 (BBCE – Baltic Biomaterials Centre of Excellence) and the Ministry of Economics Republic of Latvia project "State research project in the field of biomedicine, medical technologies, and pharmacy," project No. VPP-EM-BIOMEDICĪNA-2022/1-0001. The authors also acknowledge the help of Vahid Jahedzomorrodi in this study.

Appendix A. Supplementary data

Supplementary data to this article can be found online at https://doi.org/10.1016/j.heliyon.2024.e39753.

References

[1] S.V. Dorozhkin, M. Epple, Biological and medical significance of calcium phosphates, Angew. Chem. Int. Ed. 41 (2002) 3130–3146, https://doi.org/10.1002/1521-3773(20020902)41:17<3130::AID-ANIE3130>3.0.CO;2-1.

[2] J. Fan, K. Abedi-Dorcheh, A.S. Vaziri, F. Kazemi-Aghdam, S. Rafieyan, M. Sohrabinejad, M. Ghorbani, F.R. Adib, Z. Ghasemi, K. Klavins, et al., A review of recent advances in natural polymer-based scaffolds for musculoskeletal tissue engineering, Polymers 14 (2022), https://doi.org/10.3390/polym14102097.

[3] J.M. Bouler, P. Pilet, O. Gauthier, E. Verron, Biphasic calcium phosphate ceramics for bone reconstruction: a review of biological response, Acta Biomater. 53 (2017) 1–12, https://doi.org/10.1016/j.actbio.2017.01.076.

[4] M. Prakasam, J. Locs, K. Salma-Ancane, D. Loca, A. Largeteau, L. Berzina-Cimdina, Fabrication, properties and applications of dense hydroxyapatite: a review, J. Funct. Biomater. 6 (2015) 1099–1140, https://doi.org/10.3390/jfb6041099.

[5] S.J. Kalita, A. Bhardwaj, H.A. Bhatt, Nanocrystalline calcium phosphate ceramics in biomedical engineering, Mater. Sci. Eng. C 27 (2007) 441–449, https://doi.org/10.1016/j.msec.2006.05.018.

[6] P. Humbert, M. Brennan, N. Davison, P. Rosset, V. Trichet, F. Blanchard, P. Layrolle, Immune modulation by transplanted calcium phosphate biomaterials and human mesenchymal stromal cells in bone regeneration, Front. Immunol. 10 (2019) 1–15, https://doi.org/10.3389/fimmu.2019.00663.

[7] M. Ermis, E. Antmen, V. Hasirci, Micro and Nanofabrication methods to control cell-substrate interactions and cell behavior: a review from the tissue engineering perspective, Bioact. Mater. 3 (2018) 355–369, https://doi.org/10.1016/j.bioactmat.2018.05.005.

[8] I. Elia, M.C. Haigis, Metabolites and the tumour microenvironment: from cellular mechanisms to systemic metabolism, Nat. Metab. 3 (2021) 21–32, https://doi.org/10.1038/s42255-020-00317-z.

[9] P. Romani, L. Valcarcel-Jimenez, C. Frezza, S. Dupont, Crosstalk between mechanotransduction and metabolism, Nat. Rev. Mol. Cell Biol. 22 (2021) 22–38, https://doi.org/10.1038/s41580-020-00306-w.

[10] J. Fan, V. Jahed, K. Klavins, Metabolomics in bone research, Metabolites 11 (2021), https://doi.org/10.3390/metabo11070434.

[11] J.L. Ren, A.H. Zhang, L. Kong, X.J. Wang, Advances in mass spectrometry-based metabolomics for investigation of metabolites, RSC Adv. 8 (2018) 22335–22350, https://doi.org/10.1039/c8ra01574k.

[12] X.W. Zhang, Q.H. Li, Z. Di Xu, J.J. Dou, Mass spectrometry-based metabolomics in health and medical science: a systematic review, RSC Adv. 10 (2020) 3092–3104, https://doi.org/10.1039/c9ra08985c.

[13] D.S. Wishart, Emerging applications of metabolomics in drug discovery and precision medicine, Nat. Rev. Drug Discov. 15 (2016) 473–484, https://doi.org/10.1038/nrd.2016.32.

[14] M. Ebrahimi, M.G. Botelho, S.V. Dorozhkin, Biphasic calcium phosphates bioceramics (HA/TCP): concept, physicochemical properties and the impact of standardization of study protocols in biomaterials research, Mater. Sci. Eng. C 71 (2017) 1293–1312, https://doi.org/10.1016/j.msec.2016.11.039.

[15] R.T. Hannan, S.M. Peirce, T.H. Barker, Fibroblasts: diverse cells critical to biomaterials integration, ACS Biomater. Sci. Eng. 4 (2018) 1223–1232, https://doi.org/10.1021/acsbiomaterials.7b00244.

[16] M. Sokolova, A. Putnins, I. Kreicbergs, J. Locs, Scale-up of wet precipitation calcium phosphate synthesis, Key Eng. Mater. 604 (2014) 216–219, https://doi.org/10.4028/www.scientific.net/KEM.604.216.

[17] Z. Pang, G. Zhou, J. Ewald, L. Chang, O. Hacariz, N. Basu, J. Xia, Using MetaboAnalyst 5.0 for LC–HRMS spectra processing, multi-omics integration and covariate adjustment of global metabolomics data, Nat. Protoc. 17 (2022) 1735–1761, https://doi.org/10.1038/s41596-022-00710-w.

[18] A. Banjac, T. Perisic, H. Sato, A. Seiler, S. Bannai, N. Weiss, P. Kölle, K. Tschoep, R.D. Issels, P.T. Daniel, et al., The cystine/cysteine cycle: a redox cycle regulating susceptibility versus resistance to cell death, Oncogene 27 (2008) 1618–1628, https://doi.org/10.1038/sj.onc.1210796.

[19] L.Y. Li, S.M. Limbu, Q. Ma, L.Q. Chen, M.L. Zhang, Z.Y. Du, The metabolic regulation of dietary L-carnitine in aquaculture nutrition: present status and future research strategies, Rev. Aquacult. 11 (2019) 1228–1257, https://doi.org/10.1111/raq.12289.

[20] C. Wen, F. Li, L. Zhang, Y. Duan, Q. Guo, W. Wang, S. He, J. Li, Y. Yin, Taurine is involved in energy metabolism in muscles, adipose tissue, and the liver, Mol. Nutr. Food Res. 63 (2019) 1–11, https://doi.org/10.1002/mnfr.201800536.

[21] C.W. Cheah, N.M. Al-Namnam, M.N. Lau, G.S. Lim, R. Raman, P. Fairbairn, W.C. Ngeow, Synthetic material for bone, periodontal, and dental tissue regeneration: where are we now, and where are we heading next? Materials 14 (20) (2021) 6123, https://doi.org/10.3390/ma14206123.

[22] Pamela Habibovic, Moyo C. Kruyt, Maria V. Juhl, Stuart Clyens, Roberta Martinetti, Laura Dolcini, Naseem Theilgaard, Clemens A. van Blitterswijk, Comparative in vivo study of six hydroxyapatite-based bone graft substitutes, J. Orthop. Res. 26 (2008) 1363–1370, https://doi.org/10.1002/jor.20648.

[23] S. Hu, W. He, G. Wu, Hydroxyproline in animal metabolism, nutrition, and cell signaling, Amino Acids 54 (2022) 513–528, https://doi.org/10.1007/s00726-021-03056-x.

[24] J. Zuo, J. Tang, M. Lu, Z. Zhou, Y. Li, H. Tian, E. Liu, B. Gao, T. Liu, P. Shao, Glycolysis rate-limiting enzymes: novel potential regulators of rheumatoid arthritis pathogenesis, Front. Immunol. 12 (2021) 1–17, https://doi.org/10.3389/fimmu.2021.779787.

[25] J.A. Kelleher, P.H. Chan, T.Y.Y. Chan, G.A. Gregory, Energy metabolism in hypoxic astrocytes: protective mechanism of fructose-1,6-bisphosphate, Neurochem. Res. 20 (1995) 785–792, https://doi.org/10.1007/BF00969690.

[26] H. Li, J. Wang, H. Xu, R. Xing, Y. Pan, W. Li, J. Cui, H. Zhang, Y. Lu, Decreased fructose-1,6-bisphosphatase-2 expression promotes glycolysis and growth in gastric cancer cells, Mol. Cancer 12 (2013) 1–12, https://doi.org/10.1186/1476-4598-12-110.

[27] M.A. Razak, P.S. Begum, B. Viswanath, S. Rajagopal, Multifarious beneficial effect of nonessential amino acid, Glycine: a review, Oxid. Med. Cell. Longev. (2017), https://doi.org/10.1155/2017/1716701.

[28] E. Cheung, V. Olin-sandoval, N. Grüning, The return of metabolism: biochemistry and physiology of the pentose phosphate pathway, Biol. Rev. Camb. Phil. Soc. 90 (2015) 927–963, https://doi.org/10.1111/brv.12140.The.

[29] M.H. Soflaee, R. Kesavan, U. Sahu, A. Tasdogan, E. Villa, Z. Djabari, F. Cai, D.H. Tran, H.S. Vu, E.S. Ali, et al., Purine nucleotide depletion prompts cell migration by stimulating the serine synthesis pathway, Nat. Commun. 13 (2022) 1–14, https://doi.org/10.1038/s41467-022-30362-z.

[30] P.L. Ipata, R. Pesi, Metabolic interaction between purine nucleotide cycle and oxypurine cycle during skeletal muscle contraction of different intensities: a biochemical reappraisal, Metabolomics 14 (2018), https://doi.org/10.1007/s11306-018-1341-0, 0.

[31] D. Xu, Y. Wan, Z. Li, C. Wang, Q. Zou, C. Du, Y. Wang, Tailorable hierarchical structures of biomimetic hydroxyapatite micro/nanoparticles promoting endocytosis and osteogenic differentiation of stem cells, Biomater. Sci. 8 (2020) 3286–3300, https://doi.org/10.1039/d0bm00443j.

[32] G.E. Hansen, G.E. Gibson, The α-ketoglutarate dehydrogenase complex as a hub of plasticity in neurodegeneration and regeneration, Int. J. Mol. Sci. 23 (2022), https://doi.org/10.3390/ijms232012403.

[33] L. Zhang, Y. Yao, S. Zhang, Y. Liu, H. Guo, M. Ahmed, T. Bell, H. Zhang, G. Han, E. Lorence, et al., Metabolic reprogramming toward oxidative phosphorylation identifies a therapeutic target for mantle cell lymphoma, Sci. Transl. Med. 11 (2019) 1–17, https://doi.org/10.1126/scitranslmed.aau1167.

[34] M.P. Pandey, S. Sasidharan, V.A. Raghunathan, H. Khandelia, Molecular mechanism of hydrotropic properties of GTP and ATP, J. Phys. Chem. B (2022), https://doi.org/10.1021/acs.jpcb.2c06077.

[35] R.T. Stubbs, M. Yadav, R. Krishnamurthy, G. Springsteen, A plausible metal-free ancestral analogue of the Krebs cycle composed entirely of α-ketoacids, Nat. Chem. 12 (2020) 1016–1022, https://doi.org/10.1038/s41557-020-00560-7.
[36] B. Zdzisińska, A. Żurek, M. Kandefer-Szerszeń, Alpha-ketoglutarate as a molecule with pleiotropic activity: well-known and novel possibilities of therapeutic use, Arch. Immunol. Ther. Exp. 65 (2017) 21–36, https://doi.org/10.1007/s00005-016-0406-x.
[37] I. Martínez-Reyes, N.S. Chandel, Mitochondrial TCA cycle metabolites control physiology and disease, Nat. Commun. 11 (2020) 1–11, https://doi.org/10.1038/s41467-019-13668-3.